Initiation of primary T cell—B cell interactions and extrafollicular antibody responses in an organized microphysiological model of the human lymph node

Jonathan M. Zatorski[1]*, Djuro Raskovic[1]*, Abhinav Arneja[2], Saweetha Kiridena[1], Tochukwu Ozulumba[1], Jennifer H. Hammel[3], Parastoo Anbaei[1], Jennifer E. Ortiz-Cárdenas[1,4], Thomas J. Braciale[2], Jennifer M. Munson[3], Chance John Luckey[2], Rebecca R. Pompano[1,2,5]

* Equal contributions

[1] Department of Chemistry, 409 McCormick Road, University of Virginia, Charlottesville, VA 22904

[2] Department of Pathology, University of Virginia, Charlottesville, VA 22908

[3] Fralin Biomedical Research Institute and Department of Biomedical Engineering and Mechanics, Virginia Polytechnic Institute and State University, Roanoke, VA

[4] Stanford University, Department of Bioengineering, 443 Via Ortega, Rm 119, Stanford, CA 94305, United States

[5] Department of Biomedical Engineering, University of Virginia School of Engineering and Applied Sciences, Thornton Hall, 351 McCormick Rd, Charlottesville, VA 22904

ABSTRACT

Antibody production is central to protection against new pathogens and cancers, as well as to certain forms of autoimmunity. Antibodies often originate in the lymph node (LN), specifically at the extrafollicular border of B cell follicles, where T and B lymphocytes physically interact to drive B cell maturation into antibody-secreting plasmablasts. In vitro models of this process are sorely needed to predict aspects of the human immune response. Microphysiological systems (MPSs) offer the opportunity to approximate the lymphoid environment, but so far have focused primarily on memory recall responses to antigens previously encountered by donor cells. To date, no 3D culture system has replicated the engagement between T cells and B cells (T—B interaction) that leads to antibody production when starting with naïve cells. Here, we developed a LN-MPS to model early T—B interactions at the extrafollicular border built from primary, naïve human lymphocytes encapsulated within a collagen-based 3D matrix. Within the MPS, naïve T cells exhibited CCL21-dependent chemotaxis and chemokinesis as predicted. Naïve T and B cells were successfully skewed on chip to an early T follicular helper (pre-Tfh) and activated state, respectively, and co-culture of the latter cells led to CD38+ plasmablast cells and T cell dependent production of IgM. These responses required differentiation of the T cells into pre-Tfhs, physical cell-cell contact, and were sensitive to the ratio at which pre-Tfh and activated B cells were seeded on-chip. Dependence on T cell engagement was greatest at a 1:5 T:B ratio, while cell proliferation and CD38+ signal was greatest at a 1:1 T:B ratio. Furthermore, plasmablast formation was established starting from naïve T and B cells on-chip. We envision that this MPS model of primary lymphocyte physiology will enable new mechanistic analyses of human humoral immunity in vitro.

INTRODUCTION

The lymph node (LN) is a small organ composed of intricately organized regions of T and B lymphocytes (Figure 1a), whose interactions orchestrate a cascade of events critical for initiation of humoral immunity. In particular, T and B lymphocytes occupy adjacent and abutting zones known as the interfollicular zone and B cell follicle, respectively, which evolved to facilitate rapid responses to incoming antigens. After infection or vaccination, T cell receptor (TCR)-ligation of naïve T cells induces their differentiation into effector cells, including early T follicular helper (pre-Tfh) cells, that provide help for B cell activation (Figure 1b).[1] Pre-Tfh cells upregulate the chemokine receptor CXCR5, which enables them to migrate from the central T cell zone towards the extrafollicular region of B cell follicles.[2] Meanwhile, naïve B cells activated by inflammatory molecules upregulate expression of major histocompatibility complex class II (MHC-II),[3] and move to the B cell follicle border. Here, interactions with cognate pre-Tfh cells drive differentiation of activated B cells into plasmablasts that secrete IgM, the first class of antibody secreted in a humoral response.[4,5]. This dance of contact-dependent, multistep interactions is thought to be critical for naïve lymphocytes to generate an effective humoral response to novel antigens.

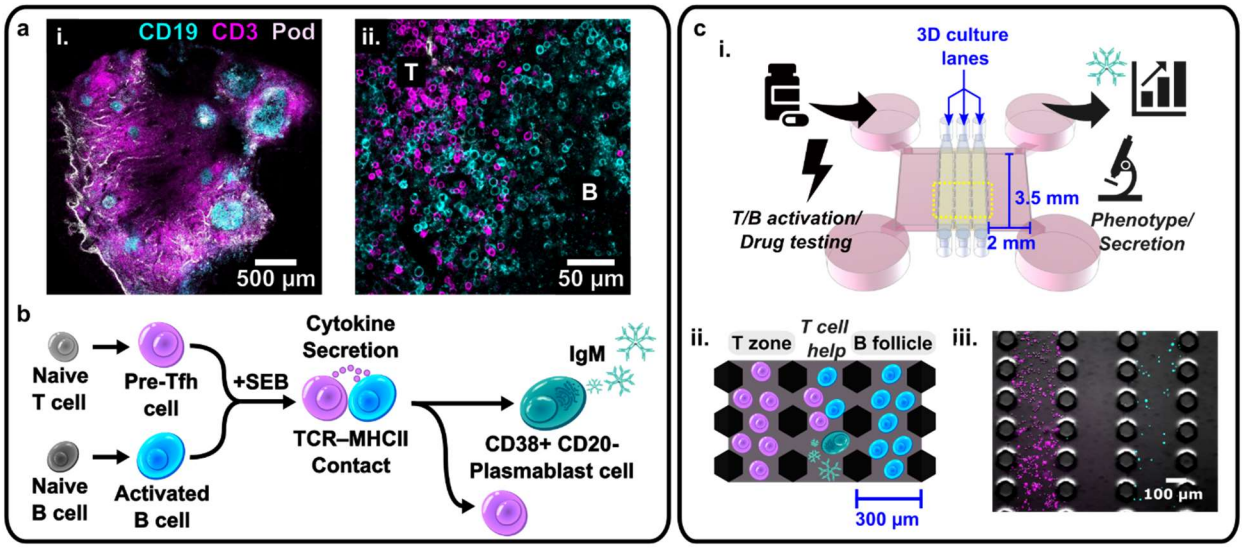

Figure 1. Modeling approach for the human LN-MPS. (a) Immunofluorescence image of a human tonsil slice (i) with magnified view of a T/B border zone (ii). FITC-anti-Podoplanin, white;

AF647-anti-CD3, magenta; PE-anti-CD19, cyan. (b) Illustration of events involved in T cell—B cell interactions in humoral immunity. Naïve T and B cells receive stimulatory signals that result in cell differentiation towards a pre-Tfh and activated B state, respectively. Pre-Tfh cells provide help to activated B cells in a TCR-MHCII-dependent manner upon exposure to cognate antigen or superantigen such as staphylococcal enterotoxin B (SEB). Activated B cells eventually mature into antibody-secreting plasmablasts. (c) Schematic of T/B border chip (not to scale) illustrating chip capabilities. (ii) Zoomed schematic and (iii) image of the 3D culture lanes, where microposts enable filling of adjacent lanes with cell-laden hydrogels via surface tension.

Unfortunately, much of the knowledge of basic LN immunology described above was derived from animal models, and it is unknown to what extent the details hold true in human tissue. Mouse and human immune signaling, though broadly conserved, differ in numerous ways that directly impact vaccine responses, including the response to TLR7/9/11 ligation,[6,7] expression of lymphocyte-attractive chemokines,[8,9] and different mechanistic roles of some cytokines, such as IL-12.[10,11] Furthermore, most clinical analysis of human immune function necessarily relies on blood draws, making it difficult to study tissue-specific cell-cell interactions. To understand the mechanisms of responses to infection, autoimmune antigens, cancer antigens, and inform the design of novel vaccines and immunotherapies, biomimetic models of human tissue immunology are critical for progress.[12,13]

Engineered in vitro models offer the potential to study these events in a tissue-like setting. As traditional 2D cultures do not easily replicate tissue-level events such as lymphocyte chemotaxis and cell-matrix interactions,[14,15] a number of 3D culture models have been developed. These cultures have replicated cell-intrinsic behaviors such as the effect of the extracellular matrix, chemokine induced cell motility and organization,[16–20] and pair-wise interactions such as dendritic cell-T cell engagement,[21–23] but models of multi-step tissue level events are rare.[24,25] For higher-order processes, organoid models based on human tonsil cells, peripheral blood mononuclear cells (PBMCs), or murine memory B cells have elegantly replicated B cell

differentiation and antibody production, sometimes in response to engagement with T cells.[26–28] However, organoid development relies on spontaneous cell clustering and thus precise control over the microenvironment is challenging; integration of immune organoids with microfluidic gradients is promising but in early stages.[28,29]

To provide additional environmental control, microphysiological systems (MPSs) offer a promising alternative. MPSs can exhibit some of the organizational and functional features of *in vivo* tissue, making them suitable for predicting mechanistic events, responses to drugs, and probing structure-function relationships.[30–33] While development of immunocompetent MPSs started over 10 years ago and has increased in the last few years, models specifically focused on the LN are more rare.[25,34,35] Exciting progress has been made in modeling T cell-dendritic cell interactions,[36] T cell-stromal cell interactions,[37,38] vaccine responses and immunosenescence,[39,40] and inflammatory and vaccine induced B cell clustering, memory B cell maturation, and antibody production.[41–43]

However, engineered lymphoid models thus far have primarily focused on antibody development from PBMCs in response to recall challenges, wherein memory cells respond to an antigen previously experienced by the donor, such as influenza or SARS-CoV-2. The focus on memory in microscale cultures is necessitated by low cell precursor frequencies, i.e. the low numbers of naïve T cells capable of recognizing a given antigen. However, while recall responses are an essential benchmark for validating T and B cell memory, they do not enable mechanistic testing of early activation or MHCII-TCR-dependent interactions between naïve T and B cells that result in antibody production. Furthermore, while mixed PBMC cultures are an excellent starting point, no lymphoid model is available to test the role of spatial organization of T and B cells on antibody production. While methods for patterning lymphocytes have been developed,[44–46] patterned immune function has not yet been demonstrated.

To address these gaps, here we describe a multi-lane microfluidic chip to model early T—B cell interactions at the extrafollicular border, starting with naïve cells and leading to antibody production (Figure 1c). The selected MPS format enabled either mixed co-cultures or patterned spatial organization, although here we primarily used it for the former. We tested the ability of the lymph node MPS (LN-MPS) to support T and B cell activation within the chamber, and to monitor chemotaxis and cytokine secretion in response to stimuli. We tested the extent to which naïve T cells were skewed to a pre-Tfh state on-chip, and tested conditions to support engagement with B cells. To overcome the low frequency of antigen specific precursors amongst naïve T and B cells, we used staphylococcal enterotoxin B (SEB), which enables polyclonal interactions by binding the TCR of T cells and MHCII receptor of B cells. We optimized the LN-MPS to mimic T cell help for B cells, which led to cluster formation, plasmablast differentiation, and antibody production. This LN-MPS advances our human experimental toolkit by enabling greater control over immune cell-cell interactions.

RESULTS

Design of the LN-MPS to provide options for mimicking lymphoid tissue spatial organization and function

When designing a LN-MPS to reproduce the activation, differentiation, and engagement of naïve T cells and B cells at the follicle border, we identified the following major design goals in terms of biological functions and analytical capabilities. Key biological functions included (a) naïve T cell activation and differentiation into cytokine-secreting pre-Tfh cells, (b) naïve B cell activation, (c) activated B cell differentiation into antibody-secreting plasmablasts, and (d) antibody production requiring T cell—B cell interactions. Required analytical capabilities included (a) control of lymphocyte organization in a 3D microenvironment, to mimic the overlap of T cell and B cell regions at the edge of the B cell follicle (Figure 1a); (b) spatial control over microenvironmental stimulation, such as to apply chemokine gradients; (c) spatially resolved

analysis of cell motility and cell-cell interactions by imaging; (d) compatibility with immunofluorescence microscopy, sampling of cell secretions, and cell recovery for downstream analysis; and (e) ease of use by biomedical scientists.

To best model the naïve, human lymphocyte population in the MPS, primary lymphocytes were isolated from human blood TRIMA collars following platelet donation. The use of TRIMA collars provided easy access to large quantities of autologous lymphocytes, and circumvented any phenotypic variation associated with iPSCs or cell lines. To ensure that the chip did not contain effector and memory cells, we isolated naïve CD4+ T and naïve B lymphocytes for use on the chip. Although it is common to culture lymphocytes in media supplemented with fetal calf serum, here we chose to use serum free media to provide greater control over early activation states.[47]

We designed the LN-MPS to mimic the 3D tissue environment by resuspending the lymphocytes in a thermally-setting collagen-fibrinogen (Coll/Fib) hydrogel.[48,49] Three parallel gel lanes were implemented to provide flexibility for experimental design. The well-established microfluidic format consists of parallel arrays of posts that provide surface-tension barriers for compartmentalized lane filling by simple pipetting (Figure 1c).[50,51] This planar design has been implemented routinely in organ-on-chip applications, is robust to use by non-experts, and is compatible with high-throughput manufacturing if needed in the future.[38,52,53] Cells could be patterned in one, two, or all three lanes, either mixed or in separate populations. Cells in the center lane could be analyzed for chemotactic responsiveness, or alternatively, cells could be patterned to mimic the organization of the B cell follicle border zone. For simplicity and improved throughput, cells were cultured in static conditions. As the three-gel-lane design is not yet available in an off-the-shelf format, we fabricated the device in PDMS with a glass bottom, which allowed for microscopic imaging as well as gas exchange.[54]

The LN-MPS supported culture and activation of naïve T cells and control over cell motility

As a first step, we tested the ability of the LN-MPS to support naïve T cell viability, activation, and chemotactic responsiveness. Purified naïve CD4+ T cells were suspended in Coll/Fib and loaded into the center lane of the chip, with the surrounding lanes filled with empty Coll/Fib (Figure 2a-b). In preliminary experiments, we found that larger gel dimensions and longer channels (3 x 800-μm-wide x 104-mm-long) caused limited gas exchange and poor viability of T cells (data not shown). Miniaturizing the chip configuration to 3 x 300-μm-wide channels (Figure 1c) and having all four reservoirs open for gas exchange resulted in on-chip viability of naïve CD4+ T cells within 80% of that of 2D plated controls after four days across multiple donors (Figure 2c). We also observed T cells had migrated into the adjacent lanes, indicating T cells were mobile (Figure 2b). Chemotactic behavior was confirmed by adding CCL21 to the left media lane; within an hour, T cells migrated out of their initial lane toward the gradient (Figure 2d-f). Furthermore, mean cell velocity was significantly higher in the presence of CCL21 (Figure 2g), consistent with prior reports of chemokinesis in response to this chemokine.[55] Finally, to assess the responsiveness of naïve CD4+ T cells to ligation of the T cell receptor (TCR) complex within the MPS, we mimicked receptor engagement by injecting a polymeric α-CD3/CD28 solution into both media lanes (Figure 2h-k). As expected, T cells were visibly larger and the early lymphocyte activation marker, CD69, was upregulated at 48 hr (Figure 2j), and IFN-γ was detected in the conditioned media from days 1 – 5 (Figure 2k). Thus, the LN-MPS supported analysis of critical functions of primary human CD4+ T cells, including culture, motility, and stimulation.

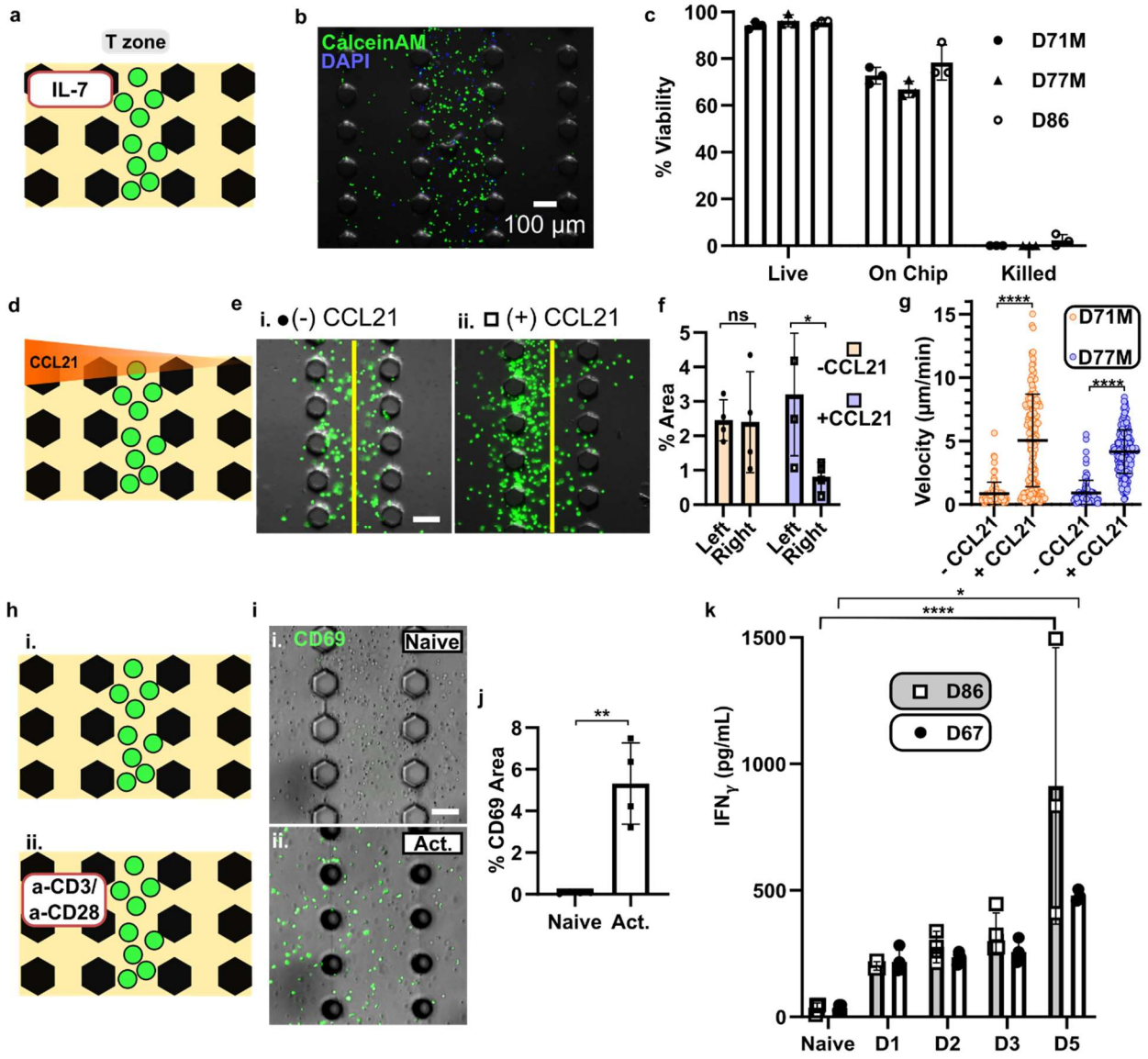

Figure 2. Naïve, CD4+ T cells were viable, responded to stimuli, and responded to chemokine CCL21 on chip. (a-c) Naïve T cells were cultured on chip with IL-7. Representative image (b) and quantification (c) of T cell viability after 4 days, labeled with (Calcein AM, green, and Dapi, blue) for 3 donors. (d-g) A CCL21 gradient was established on chip, with CCL21 added to the left-hand media lane. Representative images (e) and quantification (f) of naive CD4+ T cells after migrating toward CCL21 for 1 hr and staining with Calcein AM (green). (g) Quantification of cell velocity 30 min after gradient set up (cells were unlabeled). (h-k) Naïve T cells were cultured without (i) and with (ii) a-CD3/CD28 (StemCell). Images of CD69+ signal (FITC-anti-CD69, green) for (i) naïve and (ii) activated T cells on-chip, and quantification (j) of CD69 signal after 48 hours (unpaired T test, **:$p<0.005$). (k) Quantification of IFN-γ secretion by activated or naïve CD4+T cells on-chip measured by ELISA of supernatants collected at day 5. Panels f, g, k analyzed with ordinary two-way ANOVA with Sidak's multiple comparisons test w/single pooled variance, ns: $p>0.05$, *:$p<0.05$, ****:$p<0.00005$.

Naïve T cells differentiated into early T follicular helper cells on chip

Pre-Tfh cells are critical for support of B cell maturation and T cell-dependent antibody production. These cells are characterized by upregulation of the chemokine receptor CXCR5, regulatory protein PD-1, and the master transcription factor BCL-6 compared to naïve T cells, as well as secretion of IL-21.[2] For human cells, TCR engagement in the presence of cytokines interleukin-12 (IL-12) and activin A are capable of driving naïve T cells to Pre-Tfhs,[56] which we confirmed in 2D cultures (data not shown). Here we sought to implement pre-Tfh differentiation from naïve T cells in an MPS for the first time.

To assess skewing to a pre-Tfh phenotype, naïve CD4+ T cells were loaded into the chip and cultured for 5 days with a “skewing cocktail” composed of α-CD3/CD28, IL-12, and activin-A, added to the media lanes (Figure 3a). Cells in the skewed condition formed small clusters in the hydrogel, which were CXCR5+ by immunofluorescence staining; little CXCR5 signal was observed outside of the clusters or in the unstimulated controls (Figure 3b). T cells treated with the skewing cocktail secreted significantly more IL-21 than naive controls (Figure 3c). To further characterize the T cell state, cells were recovered from the chip after gel digestion by collagenase, and analyzed by flow cytometry (Figure 3d), which showed cells were CXCR5+, PD-1+, and BCL6+ across three donors. Thus, naïve CD4+ T cells were successfully skewed to a pre-Tfh state on chip.

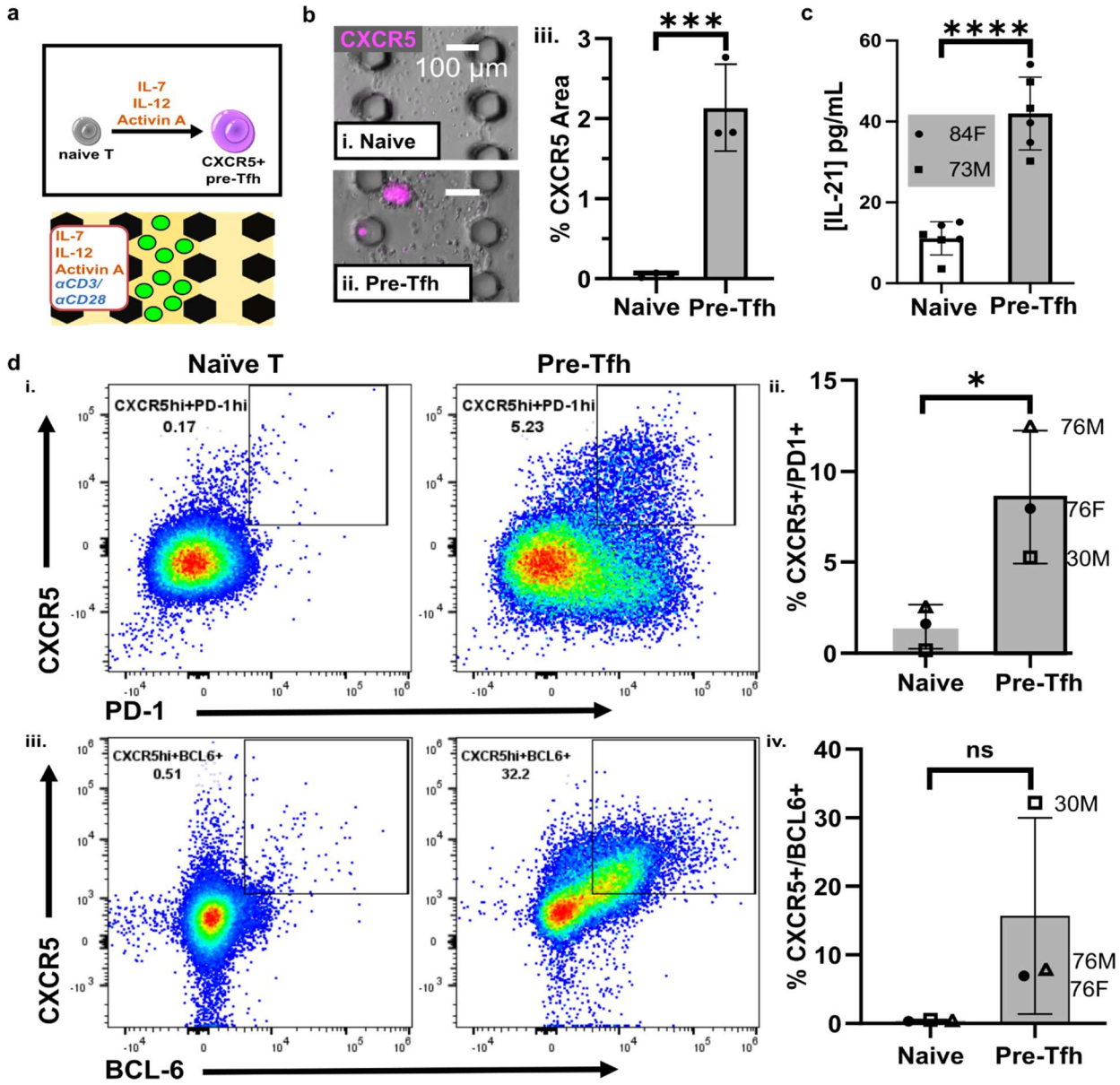

Figure 3. The LN MPS replicates human pre-Tfh development (a) Naïve T cells were cultured on-chip with anti-CD3/CD28 and a cytokine cocktail (IL-7, IL-12, and Activin A) to induce differentiation into a pre-Tfh state. (b) Overlays of immunofluorescence (AF647-anti-CXCR5, magenta) and brightfield images after 3 days culture for one representative donor, 71M, with or without Tfh-skewing cocktail (i, ii). (iii) Quantification of percent CXCR5 area across each image. Each dot shows the mean from one chip. Unpaired t test, $p<0.005$. (c) IL-21 concentration from the chip supernatants, quantified by ELISA. Unpaired t test, $p<0.001$. (d) Flow cytometry characterization of pre-Tfh markers from cells recovered from chips. (i) Flow plots with (ii) quantification of the percent of CD4+ T cells expressing CXCR5 and PD-1. (iii) Flow plots with (iv) quantification of percent of CD4+ T cells expressing CXCR5 and BCL-6. Each dot is pooled 20 chips/donor. Ratio paired T test, ns:$p>0.05$, *:$p<0.02$. Bar graphs show mean ± stdev.

Naïve B cells responded to activation stimuli on chip.

Having established the conditions for T cell culture and differentiation on the LN chip, we tested how well purified, naïve B cells could be similarly cultured and activated on chip. Activated B cells in the lymph node upregulate the activation marker CD69 and the chemokine receptor CXCR5; the latter helps them co-localize with other CXCR5+ cells, such as pre-Tfh cells.[2] To determine how well B cell activation was preserved on chip, we added a cocktail of CD40L, R848, and α-IgG/IgM (Fig 4aii). This cocktail mimics BCR ligation (α-IgG/IgM) and co-stimulation by T cells (CD40L) in an inflammatory context (R848, a TLR 7/8 agonist), as occurs after vaccination or infection. As naïve B cells exhibit a rapid decline in viability in the absence of stimulation (Figure S1), we tested culture and activation here for 48 hrs.[57] Both naïve and activated B cells remained viable for at least 48 hours on chip (Fig. 4b-d). As expected, B cells cultured with the activation cocktail appeared more blast-like (larger), and stained positivity for CD69 and CXCR5 (Fig. 4e-f). Thus, the chip supported naïve human B cells to take on an activated phenotype.

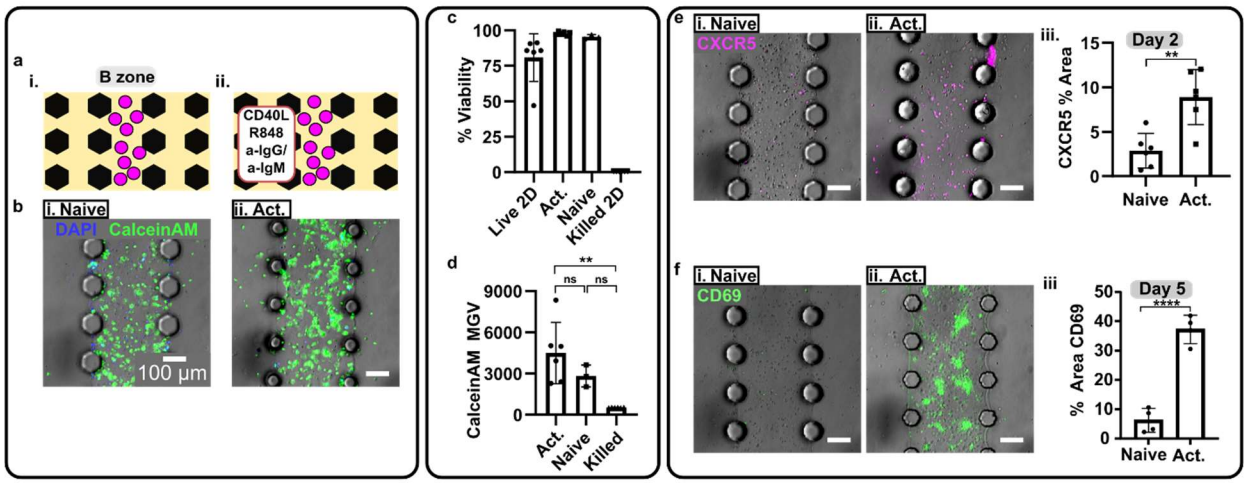

Figure 4. B cell activation on chip. (a) Schematic of naïve (i) and activated (ii) culture conditions on-chip for purified naïve CD19+ B cells. (b) Composite (fluorescence overlayed over brightfield) microscopy images of naïve (i) and activated (ii) B cells on chip with viability stain (Calcein, green, Dapi, blue) after 48 hour culture. (c) Quantification of percent viability. (d) Quantification of Calcein AM brightness across whole image. **:p<0.005, Ordinary one-way ANOVA, Tukey's multiple comparisons. (e) Images of naïve (i) and activated (ii) B cells on chip stained with AF647-anti-CXCR5 (magenta), with quantification (iii) of percent CXCR5 area across whole image, unpaired T test, **:p<0.005. (f) Images of naïve (i) and activated (ii) B cells on chip stained with FITC-anti-

CD69 (green), (iii) quantification of percent CD69 area across whole image, unpaired T test, ****:p<0.00005. Each dot is a chip. Donor information: D76M (a-e), D24F (f).

Engagement of activated B cells with pre-Tfh cells yielded antibody production in the LN-MPS

Next, we tested the extent to which the LN-MPS could predict B cell antibody secretion. We hypothesized that in the presence of SEB, pre-Tfh cells, but not naïve T cells, would provide support to activated B cells, resulting in antibody secretion. Naïve T and B cells were combined at a 1:10 ratio in 2D culture and co-cultured for three days in a B cell activating skewing cocktail (anti-IgG/IgM and R848) or B cell activating and pre-Tfh skewing cocktail (anti-IgG/IgM, R848, Activin A, IL-12, anti-CD3/CD28). To test the ability of T cells to engage the activated B cells on chip, these co-cultures were suspended in Coll/Fib and loaded onto the MPS, with or without SEB in the media, and cultured for 6 days (Figure 5a). Results from two separate donors showed that IgM was produced in large quantities (ng/mL) in the pre-Tfh—B cell co-culture conditions. Furthermore, IgM secretion was greater with pre-Tfh than with naïve T cells and was enhanced by the addition of SEB (Figure 5b), as predicted. Thus, help from pre-Tfh cells and TCR-MHCII-dependent interactions contributed to IgM secretion on the chip.

We next exploited the patterning capabilities of the LN-MPS to test the hypothesis that, in the absence of any chemokine gradients or stromal cues, pre-Tfh and activated B cells require close physical proximity to produce antibodies in vitro. Here, naïve T and B cells were skewed individually in 2D into their pre-Tfh and activated B states. Following skewing, cells were loaded onto the LN-MPS in individual outer lanes or combined in the central lane at a 1:1 ratio (Figure 5c). Once again, in the mixed population, SEB dramatically enhanced IgM secretion. Furthermore, IgM production was greater in mixed co-cultures of pre-Tfh and activated B cells than in separately patterned cell populations (Figure 5d). The combined data strongly supports the requirement of pre-Tfh help for IgM production by B cells in a TCR-MHCII-dependent manner.

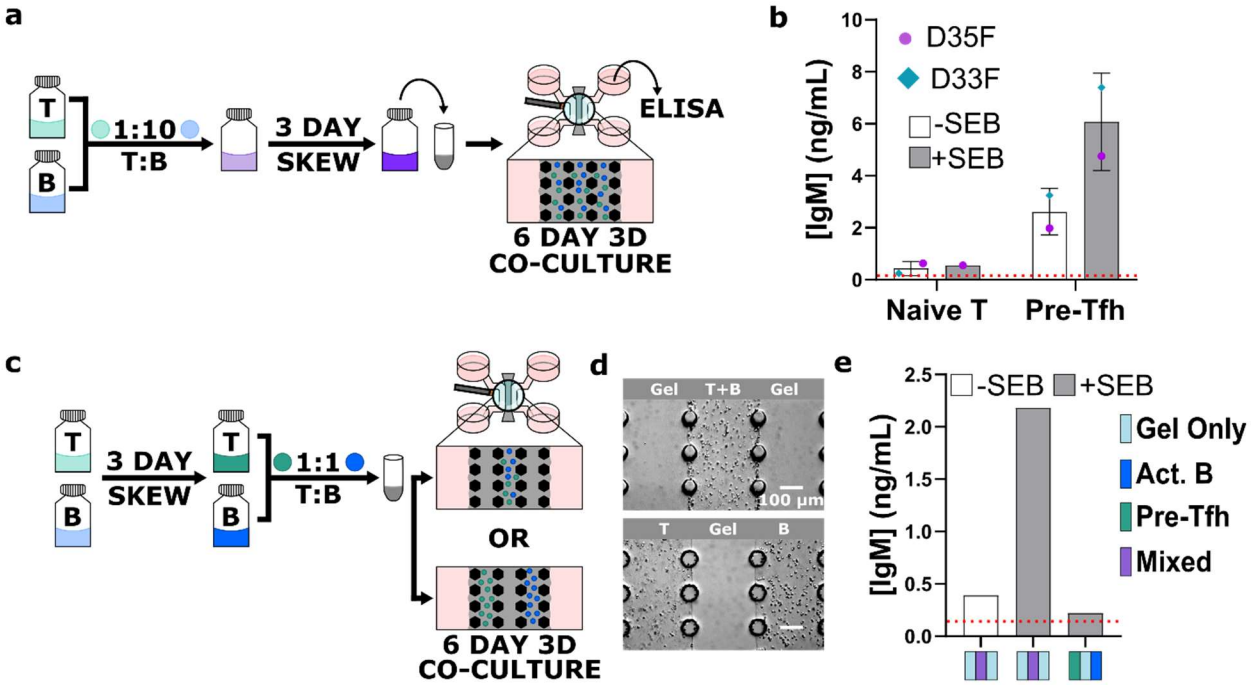

Figure 5. IgM secretion was influenced by the presence and proximity of pre-Tfh cells when co-cultured with activated B cells. (a) Schematic of experimental setup for comparing naïve T versus pre-Tfh cells and presence/absence of SEB on IgM secretion. (b) ELISA data showing IgM secretion, dots represent pooled supernatant from four chips per donor. (c) Schematic of experimental setup for analyzing IgM secretion dependency on proximity between pre-Tfh and activated B cells. (d) Brightfield images showing patterned lymphocytes on chip, day 1. (e) ELISA data showing IgM secretion. Results from four pooled chips from one donor, D68F. Red dotted lines are ELISA limit of detection: 0.140 ng/mL IgM.

CD38+ plasmablast formation and IgM production were sensitive to on-chip Tfh:B cell seeding ratios.

In classic 2D co-culture, the ratio of pre-Tfh cells to B cells significantly impacts measured outcomes.[58] As 3D culture cells have more degrees of freedom for migration and altered behavior due to matrix adhesion,[59] the optimal ratio for 3D culture was unknown. Therefore, we investigated the effect of the pre-Tfh:B cell ratio on plasmablast maturation and IgM secretion. To precisely control the ratios of these cells in the LN-MPS, we pre-skewed naïve T to pre-Tfh and naïve B to activated B cells in separate 2D cultures (off-chip), then, keeping total density constant, mixed pre-Tfh and activated B cells at ratios of 1:1, 1:5, and 1:10, respectively, in gel precursor solution.

The mixture was loaded in all three lanes of the LN-MPS (Figure 6a). Chips were cultured with or without SEB in the media, and an insulin/transferrin/selenium (ITS) supplement was added in all conditions, which we found supported T-B co-culture in 2D after inspiration from Wagar et. al.[26] (Figure S2). Interestingly, the optimal T:B ratio differed for CD38 expression and IgM secretion (Figure 6b-d). Greatest CD38+ immunofluorescent signal was measured at a 1:1 T:B ratio, whereas greatest SEB-dependent IgM production was measured at a 1:5 T:B ratio. These data are consistent with a catalytic function of pre-Tfh cells for B cells. We theorize that at 1:10 T:B cell ratios in a 3D microenvironment, B cells rarely encounter a pre-Tfh cell, and thus fail to mature into antibody-secreting plasmablasts. Meanwhile, 1:1 T-B cell ratios provide maximal support for B cell maturation towards a CD38+ plasmablast state, but the resulting high proliferation causes overcrowding and consistent cell-cell contact, resulting in loss of SEB dependence.

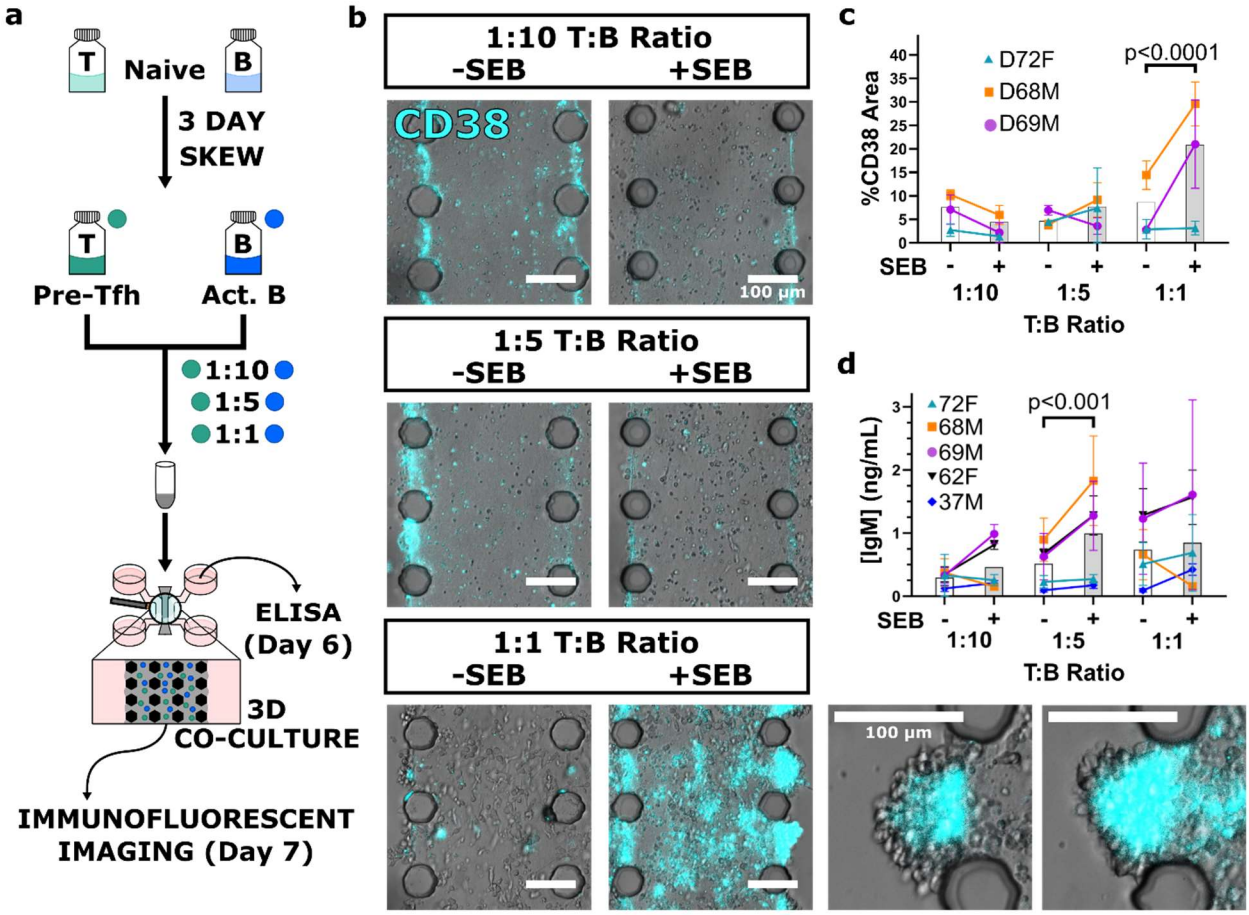

Figure 6. Cell expansion, B cell maturation, and IgM production was dependent on the T:B ratio. (a) Schematic of experimental setup. (b) Representative composite images (fluorescence overlayed over brightfield) from D69M, cells stained with AF546-anti-CD38 (cyan) on day 7. (c) Change in %CD38 positive area (3 donors). (d) IgM secretion from co-culture, quantified by ELISA on day 6. N=2-3 chips/donor (5 donors). Analyzed using two-way ANOVA with Tukey's multiple comparisons test.

$CD20^{lo}$ $CD38^{hi}$ plasmablast formation was feasible within the LN-MPS when starting with naïve T and B cells.

In all of the prior co-culture experiments, pre-Tfh and activated B cells were generated off-chip before being loaded into the LN-MPS to test their interactions in response to SEB. Here, to model the entire multi-step process that results in plasmablast production from naïve cells, we tested direct on-chip differentiation and T—B engagement in the LN-MPS. Purified naïve CD4+ T cells and naïve B cells were suspended in Coll/Fib at a 1:1 or 1:5 ratio, keeping total cell count constant, and loaded onto the chip. Cells were skewed to an activated B and pre-Tfh state for three days in 3D co-culture using a combined skewing cocktail (α-IgG/IgM, R848, IL-12, α-CD3/CD28, and Activin A). On day three, the skewing cocktail was washed out, and T—B engagement was induced by adding SEB to fresh ITS-supplemented media. Cultures without SEB were included as negative controls (Figure 7a). Cultures were visually monitored over time to allow them to reach a high density for analysis by flow cytometry, and cells were finally collected on day 16 post-skew (Figure 7b-c).

Preliminary results showed that addition of SEB increased the number of viable cells recovered for both 1:5 and 1:1 T-B ratios, with the latter having greater improvement (Figure 7d). These results demonstrate that active stimulation played a critical role in maintaining cell viability within the LN-MPS. Furthermore, in the presence of skewing media and SEB, ~35% and 38% of CD19+ B cells were $CD20^{lo}$ $CD38^{hi}$ plasmablasts at the 1:5 and 1:1 seeding ratios respectively. Plasmablast numbers were reduced by the absence of SEB (~22% at 1:5 ratio and 6% at 1:1 ratio), as expected, with higher percentages of plasmablasts generated in the 1:5 T-B ratio likely

due to the higher seeding density of B cells. Thus, it was possible to start with purified naïve T cells and B cells and progress to plasmablast differentiation on-chip in a fraction of the B cells.

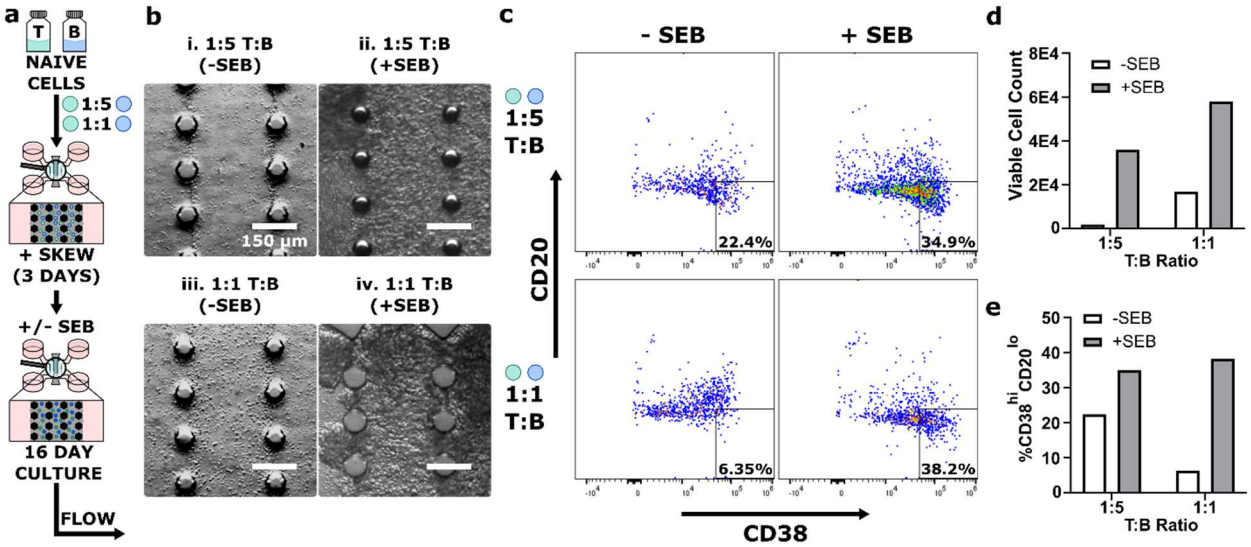

Figure 7. B cells were skewable to a plasmablast state ($CD20^{lo}$ $CD38^{hi}$) when seeded in the LN-MPS from a naïve state. (a) Schematic showing experimental setup. (b) Brightfield images showing on-chip cell density after 16 days of co-culture, post skewing. (c) Flow cytometry data for the plasmablast markers CD20 and CD38 from cells recovered from chips. Plots were gated on CD19+ B cells. (d) Total live cell count as determined by flow cytometry. (e) Percent $CD20^{lo}$ $CD38^{hi}$ plasmablast cells recovered from on-chip cultures. One donor, D39M, 5-6 pooled chips/condition.

CONCLUSION

Here we present a primary human LN-MPS to model T cell—B cell interactions at the B cell extrafollicular border, designed to be easy-to-use without pumps and compatible with brightfield and fluorescence imaging. Using naïve CD4+ T cells and B cells isolated from blood, the model reproduced expected functions of T cells and B cells, including chemokinesis and chemotaxis of naïve T cells towards a CCL21 chemokine gradient, skewing of naïve T cells towards a pre-Tfh state, and activation of naïve B cells. This system successfully replicated IgM production by B cells in a TCR-MHCII-dependent manner, and IgM production required both the presence of pre-Tfh cells and their close spatial proximity to activated B cells. We showed that a

traditional 1:10 T:B co-culture ratio from 2D cultures was insufficient for significant plasmablast generation or antibody production in a 3D culture system that enables greater degrees of freedom for cell movement. Rather, for a week-long co-culture, a 1:5 T:B ratio was required for TCR-MHCII-dependent IgM production, and 1:1 T:B ratio was required for maximal cell proliferation and CD38+ plasmablast generation. Finally, the LN-MPS successfully modeled cell-cell interactions, starting with naïve T and B cells, leading towards $CD20^{lo}$ $CD38^{hi}$ plasmablast formation; a multi-step process fundamental for generating effective humoral responses.

The current system has several limitations that present opportunities for further advancement. The LN-MPS successfully modeled T cell chemotaxis towards CCL21, but due to the small length scale and typical rates of protein diffusion, gradients are intact for <3 hour prior to equilibration. Long-term gradient maintenance in microfluidic systems is traditionally accomplished by maintaining constant fluid flow. Alternatively, biochemical sources and sinks could be introduced, which could also provide greater control over spatial distribution. Furthermore, the lack of fluid flow, although it enables easy scaling of the system to dozens or hundreds of chips simultaneously, prevents the study of shear-mediated effects of interstitial fluid flow in this system. Future integration with scalable pumping would address these areas when needed. Finally, while the current system showed TCR-MHCII-dependent IgM production, we failed to detect IgG levels in the cell supernatants above the baseline levels of IgG in AIM-V media (Figure S3). We believe that this suggests additional biological cues may be required for skewed pre-Tfh cells to induce activated B cells to class switch and produce IgG. Stromal cells and antigen presenting cells were omitted here for simplicity, but future studies including these cells are warranted to determine the cellular and molecular requirements for human class-switching in this system.

With its current focus on predicting IgM responses from naïve lymphocytes as well as with future expansions of the system, we envision that the current LN-MPS will enable many future

investigations into human immunity. Differences in immune function and regulation between cells drawn from varying donor age groups, sexes, body masses, and other biological factors that are currently poorly studied can easily be evaluated in future studies using this system. In addition, the system is well suited to test the impact of immunostimulatory and suppressant drugs on T cell—B cell interactions and IgM production, both for drug testing and toxicology. Furthermore, mechanistic experiments to probe the role of organization at a tissue-level scale are feasible due to control over cell placement in various lanes, seeding ratios, densities, and gradients of soluble factors within the LN-MPS, coupled with the ability to image on chip or collect samples for downstream analysis. The system may also be coupled with other organ-on-chip systems to study the impact of upstream organs on T—B interactions, thus ultimately serving as a tool for modeling antibody production, mechanisms of immunological dysfunction, or toxicology in diverse human populations.

METHODS

Immunostaining and imaging of tonsil slices

Male and female human tonsils were provided by the UVA Biorepository and Tissue Research Facility as de-identified surgical discard tissue. The tonsil tissue was cleaned to remove portions damaged by surgery, and a 3 mm biopsy punch was used to obtain smaller pieces (Sigma Aldrich), 300-μm-thick tissue slices were collected and labelled for live immunofluorescence imaging according to procedures previously developed for murine lymph node tissues, with minor modifications as follows.[60,61] Briefly, the small tonsil pieces were embedded in 6% w/v low melting point NuSieve GTG agarose (Lonza) in 1× PBS without calcium or magnesium (Gibco) and punched out with a 10-mm biopsy punch. The agarose was sterilized by autoclaving prior to embedding tissue for sterile slicing. The embedded tissue was sliced to 300 μm thickness using a Leica VT1000S vibratome (Leica) set to a frequency of 6 (60 Hz), amplitude of 5 (1 mm), and speed of 3.9 (~0.153 mm/s). Immediately after slicing, the tissue slices

were placed in sterile “RMPI complete media” composed of RPMI (Lonza, Maryland, USA) supplemented with 10% FBS (Corning, New York, USA), 1X L-glutamine (Gibco Life Technologies, Maryland, USA), 50 U/mL Pen/Strep (Gibco Life Technologies, Maryland, USA), 50 μM beta-mercaptoethanol (Gibco Life Technologies, Maryland, USA), 1 mM sodium pyruvate (Hyclone, Utah, USA), 1X non-essential amino acids (Hyclone, Utah, USA), and 20 mM HEPES (VWR, Pennsylvania, USA) 1X Normocin (InvivoGen, California, USA) and incubated in a cell culture incubator for at least 1 hour before staining. Figure a(i) tonsil came from unknown donor, and a(ii) tonsil came from a 3 year old male African American/Non-Hispanic donor.

Following incubation, the tonsil slices were transferred to a Parafilm-covered surface, and a stainless-steel washer was placed on top. The tonsil tissue slices were treated with 25 μg/mL of anti-mouse CD16/32 in media for 30 minutes in a cell culture incubator. After blocking, 40 μg/mL fluorescently labeled antibody cocktail prepared in media was added to the slices, and they were incubated for an additional hour in the cell culture incubator. Finally, the stained tonsil slices were washed by immersion in sterile media for at least 30 min in a cell culture incubator before imaging. Tonsil slice imaging was performed on an upright Nikon A1Rsi confocal microscope, using 400, 487, 561 and 638 nm lasers with 450/50, 525/50, 600/50 and 685/70 nm GaAsP detectors, respectively. Images were collected with 4x and 40x/0.45NA Plan Apo NIR WD objectives. Image analysis was completed using ImageJ software 1.48v.

Cell sourcing and culture media

Naïve, human CD4+ T cells and naïve B cells were purified from TRIMA collars, a derivative product of platelet apheresis. Donors were healthy and de-identified, with age and gender information reported (StemCell Technologies, Crimson Core, Brigham and Women's Hospital, Boston, MA and INOVA Laboratories, Sterling, VA). Donor codes shown throughout the paper are “D” (for donor), “Age,” “Sex” (M/F, when reported). For example a 77-year-old, female

donor would be assigned the code “D77F.” Cells were purified using negative isolation. Briefly, whole blood from TRIMA collars was collected and diluted to a total volume of 30 mL using a 1X PBS 2% heat inactivated FBS solution. Diluted whole blood was evenly split and total T and B cell populations were enriched according to manufacturer protocol using RosetteSep Human T Cell Enrichment Cocktail (StemCell Technologies, Cat#15061) and RosetteSep Human B cell Enrichment Cocktail (StemCell Technologies, Cat#15024), respectively. Following incubation, blood was further diluted to 35 mL total volume as previously described, overlayed over 15 mL of Ficoll-Paque Premium density gradient media, density 1.078 g/mL, (Cytiva, USA, Cat#17544202) and centrifuged at 1200G for 20 minutes with break off. Following centrifugation, the top 25 mL of the plasma layer was discarded. The remaining plasma layer, interphase layer, and density gradient media layer was collected, leaving coagulated pellet undisturbed. Collected solutions were washed twice and resuspended in 1X PBS, 2% heat inactivated FBS, and 1 mM EDTA in preparation for naïve cell isolation. Naïve CD4+ T and CD19+ B cell populations were isolated using EasySep Human Naïve CD4+ T cell Isolation Kit (StemCell, Cat#19555) and EasySep Human Naïve B Cell Isolation Kit (StemCell, Cat#17254) following manufacturer protocols. Analysis of isolation efficiency by flow cytometry confirmed on average >90% pure naïve CD4+ T cells and >90% pure naïve CD19+ B cells were isolated.

Cells were cultured in serum-free AIM-V media containing phenol red pH indicator, L-glutamine, 50 µg/mL streptomycin sulfate and 10 µg/mL gentamicin sulfate (Gibco, P/N 12055083). In 2D culture, T and B lymphocytes were cultured at 1-3 x 10^6 cells/mL. For maintaining viable naïve CD4+ T cells, IL-7 was added at a concentration of 4 ng/mL. To activate naïve CD4+ T cells in 2D and 3D culture, ImmunoCult™ Human CD3/CD28 T Cell Activator (StemCell Technologies) was added to the media at a concentration of 25 µL/mL media. For Tfh skewing, naïve CD4+T cells were activated with ImmunoCult™ and cultured with IL-12 (5 ng/mL) and activin A (100 ng/mL) (R&D Systems). To activate naïve B cells in monoculture, a cocktail of

human α-IgG/IgM (10 μg/mL) (Affinipure Goat Antihuman IgG+IgM (H+L), Jackson ImmunoResearch), R848 (500 μg/mL) (Invivogen), and CD40 ligand (100 μg/mL) was added to the culture media. When B cells were activated in co-culture with T cells, CD40 ligand was not added to the cocktail. Staphylococcus enterotoxin B (SEB) (Toxin Technology) was added at a concentration of 1 μg/mL.

Hydrogel preparation

Collagen/fibrinogen hydrogel was prepared by diluting 5 mg/mL rat tail I collagen (Ibidi) and 2 mg/mL fibrinogen (Sigma Aldrich) in 1x PBS. The pH was adjusted to 7.4 while on ice, according to the Ibidi protocol for preparation of collagen gels, to a final concentration of 1.5 mg/mL collagen and 1 mg/mL fibrinogen. For experiments involving T or B lymphocytes in isolation on chip, cells were resuspended in hydrogel at 1.0×10^7 cells/mL. For experiments with T/B co-cultures, cells were resuspended in hydrogel at a density of 2.5×10^7 cells/mL.

Microfluidic chip design and fabrication

The microfluidic housing used for the LN MPS was fabricated from a thin layer of polydimethylsiloxane (PDMS) patterned by standard soft lithography and irreversibly bonded to a 50 x 75 mm glass slide.[44] The PDMS microchamber was comprised of five parallel channels separated by arrays of hexagonal micropillars (100 μm in vertex-to-vertex diameter, with 50 μm spacing between pillars). The outer channels each had 8-mm diameter inlets and outlets that served as media reservoirs, while the inner gel channels had 0.75-mm inlets and outlets. Excluding the converging, angled channel regions, the media lanes were 2.05 x 0.13 x 3.5 mm^3, and the gel lanes were 0.3 x 0.13 x 3.5 mm^3. A schematic is included in the supplemental information (Figure S4).

Viability staining on chip

Viability staining was performed by first removing bulk media from the media reservoirs and rinsing each side of the chip with 150 μL of 1X PBS. Bulk rinsate was removed from the wells and 150 μL of 10 μM Calcein AM and 1 μM DAPI solution in 1X PBS was added to each side of the chip (Fisher Scientific). Chips were placed in a cell culture incubator for 1 hr. The media reservoirs were then rinsed twice with excess (500 μL) PBS, once every thirty minutes, for 1 hr., and then imaged immediately.

Chemotaxis measurement on chip

For assessing chemotactic activity of naïve CD4+ T cells on chip, a solution of 0.1 μM CCL21 (recombinant human, Peprotech, NJ, USA, Cat# 300-35A) in AIMV media was added to the left media reservoir. The chip was incubated in a cell culture incubator for 30 min for assessing live-cell motility or 1 hr for assessing total cell displacement. Cells were imaged using brightfield microscopy (no labeling) for live-cell imaging, and cells were labeled with 10 uM Calcein AM prior to imaging for total cell displacement. To perform live-cell motility imaging, chips were imaged on a stage-top incubator set to 37 C at 30 sec intervals for 5 min. For calculating mean cell velocity, individual cells were tracked using CellTracker ver.1.1 with semi-automated tracking; matching modality was set to histogram matching, maximal cell displacement was set to 20, and cell diameter was set to 40.[62]

Immunofluorescence staining on chip

For immunofluorescence staining on chip, the bulk culture media was removed from the media reservoirs and the chip was rinsed with 150 μL of 1X PBS. Bulk rinsate was removed from the wells and 100 μL of the appropriate antibody cocktail prepared in Hanks Buffered Saline Solution (ThermoFisher, Cat# 14025092) was placed in the top media reservoirs. Antibody information is available in Table S1. Antibody cocktail was allowed to flow to the bottom media reservoirs via gravity-driven flow. Cells were stained for 1 hr. while incubating at 37 °C, and then

the media reservoirs were rinsed first with HBSS for 20 min. and then twice with AIM-V media for 20 min. prior to imaging.

Microscopy of the LN MPS

All microscopy performed within the LN MPS was done using either a ZEISS AxioZoom.V16 or ZEISS AxioObserver Inverted. The AxioZoom.V16 was fitted with a HXP 200C metal halide illumination source, PlanNewFluor Z 1X objective (0.25 NA, FWD 56 mm), and an Axiocam 506 mono camera. Fluorescence imaging used Zeiss Filter Sets 38 HE (Ex: 470/40, Em: 525/50); 43 (Ex: 550/25, Em: 605/70); 49 HE (Ex: 365, Em: 445/50); 64 HE (Ex: 587/25, Em: 647/70); and brightfield images collected using transmitted light. The AxioObserver Inverted was fitted with a Colibri.7 LED light source, LD PN 20X objective (0.4 NA, FWD 7.9 mm), and ORCA-Flash4.0 LT + sCMOS camera (Hamamatsu). Transmitted light was used for collecting brightfield images and a ZEISS 112 HE LED penta-band filter was used for acquiring fluorescent images. Zen 3 Blue software was used for image collection. Image analysis was completed using ImageJ software 1.48v.

Cytokine and antibody secretion detection

All cytokines and antibodies were detected by sandwich ELISA in a high binding 96-well plate (Fisher Healthcare, Cat# 07-200-37). IgM was detected using a Human IgM ELISA Antibody Pair Kit (StemCell technologies, Cat#01995), and IL-21 was detected using an ELISA Flex: Human IL-21 (HRP) kit (Mabtech, Ohio, USA, Cat#3540-1H-6) following manufacturer protocols. IFN-γ was detected using an in-house optimized ELISA assay. Briefly, unconjugated mouse monoclonal anti-human IFN-γ (clone NIB42) was used as the capture antibody, recombinant human IFN-γ (peprotech, Cat# 300-02) was used as the standard, and biotinylated mouse monoclonal anti-human IFN-γ (clone 4S.B3) was used as the detection antibody. 150 µL/well ELISA wash buffer (1% BSA, 0.05% TWEEN-20, 1X PBS) was used to rinse plates in-between all steps. 150 µL/well blocking buffer (1% BSA, 1X PBS) was used to block plates, and all other

reagents were added at 50 µL/well. Well plates were incubated overnight at 4 °C using 1 µg/mL capture antibody in 1X PBS. Following rinsing (3X), plates were blocked with ELISA block buffer for 1 hour at room temperature. Plates were rinsed again (3X) and samples and standards were added to the plate for a 1.5 hr. room-temp incubation. Detection antibody was prepared at 0.5 µg/mL in ELISA block buffer, added after rinsing (3X), and incubated for 1.5 hrs. at room temp. Avidin-HRP (biolegend, Cat# 405103) was diluted in ELISA block buffer at a 1:500 ratio, added to the plate following rinsing (3X), and incubated for 30 min. at room temperature, in the dark. The plate was then rinsed again (5X) and TMB substrate (Fisher Healthcare, Cat# BDB555214) was added to the plate, and incubated in the dark until a color gradient across the standard wells was observed, no more than 10 min. The TMB-HRP reaction was stopped using 1M H_2SO_4 and absorbance readings taken at 450 nm on a plate reader (BMG Labtech Clariostar).

Cell recovery for flow cytometric analysis

To recover cells, collagenase D (1 mg/mL in PBS) (Sigma Aldrich) was added to the media lanes and incubated at 37 °C for fifteen minutes. Following digestion, the elastic PDMS housing was massaged with a pipette tip to break up the internal 3D cell culture. Finally, an ice-cold solution 2% FBS in 1X PBS was used to rinse across the media lanes. To recover enough cells for analysis, cells were pooled from up to twenty chips from a single donor, as indicated in the figure captions.

Flow cytometry

Cells were incubated with the fixable viability dye efluor 780 (eBioscience, ThermoFisher Scientific) according to manufacturer's instructions to determine the overall viability of lymphocytes in culture. To assess the differentiation state of T and B lymphocytes, cells were suspended in FACS staining buffer (PBS + 2% FBS—Heat Inactivated + 0.1% Sodium Azide) and first stained with biotin-conjugated rat anti-human CXCR5 antibody (Clone: RF8B2, BD Biosciences). After staining with anti-CXCR5 antibody, the cells were stained with the following

fluorescently conjugated reagents: Brilliant Violet 421 conjugated streptavidin, anti-human CD69 (FITC), anti-human CD4 (PE-Cy7), anti-human CD38 (PE), anti-human CD19 (Alexa Fluor 647), anti-human PD-1 (Brilliant Violet 711), and anti-human CD20 (Brilliant Violet 510). All the previously listed antibodies were purchased from Biolegend.

For intracellular staining, cells were fixed and permeabilized after staining for surface antigens using the Foxp3 intracellular staining kit (eBioscience, ThermoFisher Scientific) according to manufacturer's instructions. Permeabilized cells were then stained with either Alexa Fluor 647 conjugated mouse anti-human BCL6 (clone: K112-91, BD Biosciences) or mouse IgG1,κ isotype control (Biolegend).

Stained cells were acquired using the Attune NXT flow cytometer (ThermoFisher Scientific) and flow cytometry data were analyzed using FlowJo software (BD Biosciences) and GraphPad Prism.

Pre-Tfh cells were defined as $CD4^{+}CXCR5^{hi}PD\text{-}1^{hi}$ (surface expression) or $CD4^{+}CXCR5^{hi}BCL6^{hi}$ cells (intracellular staining), and plasmablasts were defined as having a surface expression phenotype of $CD19^{+}CD38^{hi}CD20^{lo}$ cells.

Statistical analysis

Graphs, line-fitting, and statistical analysis was prepared using GraphPad Prism 8.4.2.

AUTHOR CONTRIBUTIONS

JMZ, DR, AA, TO, JOC, CJL, JMM, and RRP led the experimental design and interpreted the findings. JMZ, DR, AA, SK, TO, PA, and RRP drafted the manuscript. JMZ designed and produced the microfluidic device and related experiments for 3D culture, manipulation, and characterization of lymphocytes. AA designed lymphocyte culture protocols, isolated and performed culture experiments with lymphocytes in 2D, and designed and performed all flow cytometry characterization experiments. DR designed and conducted the co-culture experiments

on chip, with technical assistance from SK. DR and TO contributed to experimental set-up and data collection, and performed ELISAs. PA performed tonsil slicing and its immunofluorescence staining and imaging. JMM provided tissue engineering and tissue analysis expertise and edited the manuscript. CJL provided immunology expertise regarding lymphocyte isolation, activation, and co-culture. TJB provided immunology expertise regarding the various strategies for activating lymphocytes. The manuscript was critically revised by all authors with the exception of TJB, who sadly passed away prior to completion of this study.

DECLARATION OF COMPETING INTEREST

JOC and RRP are listed as inventors on a patent application (Serial No. 17/045,459) filed by the University of Virginia related to spatially patterned lymph node organ-on-chip systems. All other authors declare that they have no competing financial interests or personal relationships that could have appeared to influence the work reported in this paper.

ACKNOWLEDGEMENTS

This work was supported by the National Institute of Biomedical Imaging and Bioengineering (NIBIB), with co-funding from the National Center for Advancing Translational Sciences (NCATS) at the National Institutes of Health (NIH), under Award Number U01EB029127. JMZ was supported in part by the National Science Foundation Graduate Research Fellowship Program (NSF GRFP). TO was supported in part by a Summer Research Award through the Global Infectious Diseases Institute at the University of Virginia. PA was supported by the National Institute of Allergy and Infectious Diseases under Award Number R01AI131723. JOC was supported in part by the NIH-funded T32 Biotechnology Training Program at the University of Virginia. JHH was supported by the Institute for Critical Technology and Applied Science (ICTAS) at Virginia Tech.

SUPPLEMENTARY DATA

Please see the SI document for supporting formation which includes Figure S1. Naïve T and B cell viability over time with and without cytokine supplementation, Figure S2. ITS and ITS-X supplements improve cell viability in T-B co-cultures, Figure S3. Neat AIM-V media has significant IgG background, Figure S4. Schematic of the T-B border chip, Tabel S1. List of antibodies used to label cells for fluorescent microscopy, and supporting references.

REFERENCES

(1) Murphy, K.; Weaver, C. *Janeway's Immunobiology*; Garland Science, 2016.
(2) Crotty, S. T Follicular Helper Cell Biology: A Decade of Discovery and Diseases. *Immunity* **2019**, *50* (5), 1132–1148.
(3) Su, K.-Y.; Watanabe, A.; Yeh, C.-H.; Kelsoe, G.; Kuraoka, M. Efficient Culture of Human Naive and Memory B Cells for Use as APCs. *J. Immunol.* **2016**, *197* (10), 4163–4176. https://doi.org/10.4049/jimmunol.1502193.
(4) Willard-Mack, C. L. Normal Structure, Function, and Histology of Lymph Nodes: *Toxicol. Pathol.* **2016**. https://doi.org/10.1080/01926230600867727.
(5) Sathe, A.; Cusick, J. K. Biochemistry, Immunoglobulin M. In *StatPearls*; StatPearls Publishing: Treasure Island (FL), 2025.
(6) Honda, K.; Ohba, Y.; Yanai, H.; Negishi, H.; Mizutani, T.; Takaoka, A.; Taya, C.; Taniguchi, T. Spatiotemporal Regulation of MyD88–IRF-7 Signalling for Robust Type-I Interferon Induction. *Nature* **2005**, *434* (7036), 1035–1040. https://doi.org/10.1038/nature03547.
(7) López-Yglesias, A. H.; Camanzo, E.; Martin, A. T.; Araujo, A. M.; Yarovinsky, F. TLR11-Independent Inflammasome Activation Is Critical for CD4+ T Cell-Derived IFN-γ Production and Host Resistance to Toxoplasma Gondii. *PLOS Pathog.* **2019**, *15* (6), e1007872. https://doi.org/10.1371/journal.ppat.1007872.
(8) Manzo, A.; Paoletti, S.; Carulli, M.; Blades, M. C.; Barone, F.; Yanni, G.; Fitzgerald, O.; Bresnihan, B.; Caporali, R.; Montecucco, C.; Uguccioni, M.; Pitzalis, C. Systematic Microanatomical Analysis of CXCL13 and CCL21 in Situ Production and Progressive Lymphoid Organization in Rheumatoid Synovitis. *Eur. J. Immunol.* **2005**, *35* (5), 1347–1359. https://doi.org/10.1002/eji.200425830.
(9) Carlsen, H. S.; Haraldsen, G.; Brandtzaeg, P.; Baekkevold, E. S. Disparate Lymphoid Chemokine Expression in Mice and Men: No Evidence of CCL21 Synthesis by Human High Endothelial Venules. *Blood* **2005**, *106* (2), 444–446. https://doi.org/10.1182/blood-2004-11-4353.
(10) Mestas, J.; Hughes, C. C. W. Of Mice and Not Men: Differences between Mouse and Human Immunology. *J. Immunol.* **2004**, *172* (5), 2731–2738. https://doi.org/10.4049/jimmunol.172.5.2731.
(11) Hunter, C. A. New IL-12-Family Members: IL-23 and IL-27, Cytokines with Divergent Functions. *Nat. Rev. Immunol.* **2005**, *5* (7), 521–531. https://doi.org/10.1038/nri1648.
(12) Davis, M. M. A Prescription for Human Immunology. *Immunity* **2008**, *29* (6), 835. https://doi.org/10.1016/j.immuni.2008.12.003.
(13) Farber, D. L. Tissues, Not Blood, Are Where Immune Cells Function. *Nature* **2021**, *593* (7860), 506–509. https://doi.org/10.1038/d41586-021-01396-y.

(14) Kobayashi, Y.; Watanabe, T. Gel-Trapped Lymphorganogenic Chemokines Trigger Artificial Tertiary Lymphoid Organs and Mount Adaptive Immune Responses In Vivo. *Front. Immunol.* **2016**, *7*, 316. https://doi.org/10.3389/fimmu.2016.00316.
(15) Luther, S. A.; Bidgol, A.; Hargreaves, D. C.; Schmidt, A.; Xu, Y.; Paniyadi, J.; Matloubian, M.; Cyster, J. G. Differing Activities of Homeostatic Chemokines CCL19, CCL21, and CXCL12 in Lymphocyte and Dendritic Cell Recruitment and Lymphoid Neogenesis1. *J. Immunol.* **2002**, *169* (1), 424–433. https://doi.org/10.4049/jimmunol.169.1.424.
(16) Grandhi, T. S. P.; Mebrahtu, M.; Musso, R.; Fullman, A.; Nifong, B.; Wisdom, K.; Roh, T. T.; Sender, M.; Poore, D.; Macdougall, C. E.; Oren, R.; Griffin, S.; Cheng, A. T.; Ekert, J. E. A Microphysiological Assay for Studying T-Cell Chemotaxis, Trafficking and Tumor Killing. *Biofabrication* **2024**, *17* (1), 015004. https://doi.org/10.1088/1758-5090/ad847f.
(17) Sadjadi, Z.; Zhao, R.; Hoth, M.; Qu, B.; Rieger, H. Migration of Cytotoxic T Lymphocytes in 3D Collagen Matrices. *Biophys. J.* **2020**, *119* (11), 2141–2152. https://doi.org/10.1016/j.bpj.2020.10.020.
(18) Pruitt, H. C.; Lewis, D.; Ciccaglione, M.; Connor, S.; Smith, Q.; Hickey, J. W.; Schneck, J. P.; Gerecht, S. Collagen Fiber Structure Guides 3D Motility of Cytotoxic T Lymphocytes. *Matrix Biol. J. Int. Soc. Matrix Biol.* **2019**. https://doi.org/10.1016/j.matbio.2019.02.003.
(19) Valignat, M.-P.; Theodoly, O.; Gucciardi, A.; Hogg, N.; Lellouch, A. C. T Lymphocytes Orient against the Direction of Fluid Flow during LFA-1-Mediated Migration. *Biophys. J.* **2013**, *104* (2), 322–331. https://doi.org/10.1016/j.bpj.2012.12.007.
(20) Tomei, A. A.; Siegert, S.; Britschgi, M. R.; Luther, S. A.; Swartz, M. A. Fluid Flow Regulates Stromal Cell Organization and CCL21 Expression in a Tissue-Engineered Lymph Node Microenvironment. *J. Immunol. Baltim. Md 1950* **2009**, *183* (7), 4273–4283. https://doi.org/10.4049/jimmunol.0900835.
(21) Sapudom, J.; Alatoom, A.; Mohamed, W. K. E.; Garcia-Sabaté, A.; McBain, I.; Nasser, R. A.; Teo, J. C. M. Dendritic Cell Immune Potency on 2D and in 3D Collagen Matrices. *Biomater. Sci.* **2020**, *8* (18), 5106–5120. https://doi.org/10.1039/D0BM01141J.
(22) Abu-Shah, E.; Demetriou, P.; Bálint, Š.; Mayya, V.; Kutuzov, M. A.; Dushek, O.; Dustin, M. L. A Tissue-like Platform for Studying Engineered Quiescent Human T-Cells' Interactions with Dendritic Cells. *eLife* **2019**, *8*, e48221. https://doi.org/10.7554/eLife.48221.
(23) Stachowiak, A. N.; Irvine, D. J. Inverse Opal Hydrogel-Collagen Composite Scaffolds as a Supportive Microenvironment for Immune Cell Migration. *J. Biomed. Mater. Res. A* **2008**, *85* (3), 815–828. https://doi.org/10.1002/jbm.a.31661.
(24) Hammel, J. H.; Zatorski, J. M.; Cook, S. R.; Pompano, R. R.; Munson, J. M. Engineering in Vitro Immune-Competent Tissue Models for Testing and Evaluation of Therapeutics. *Adv. Drug Deliv. Rev.* **2022**, 114111. https://doi.org/10.1016/j.addr.2022.114111.
(25) Ozulumba, T.; Montalbine, A. N.; Ortiz-Cárdenas, J. E.; Pompano, R. R. New Tools for Immunologists: Models of Lymph Node Function from Cells to Tissues. *Front. Immunol.* **2023**, *14*, 1183286. https://doi.org/10.3389/fimmu.2023.1183286.
(26) Wagar, L. E.; Salahudeen, A.; Constantz, C. M.; Wendel, B. S.; Lyons, M. M.; Mallajosyula, V.; Jatt, L. P.; Adamska, J. Z.; Blum, L. K.; Gupta, N.; Jackson, K. J. L.; Yang, F.; Röltgen, K.; Roskin, K. M.; Blaine, K. M.; Meister, K. D.; Ahmad, I. N.; Cortese, M.; Dora, E. G.; Tucker, S. N.; Sperling, A. I.; Jain, A.; Davies, D. H.; Felgner, P. L.; Hammer, G. B.; Kim, P. S.; Robinson, W. H.; Boyd, S. D.; Kuo, C. J.; Davis, M. M. Modeling Human Adaptive Immune Responses with Tonsil Organoids. *Nat. Med.* **2021**, *27* (1), 125–135. https://doi.org/10.1038/s41591-020-01145-0.
(27) Graney, P. L.; Zhong, Z.; Post, S.; Brito, I.; Singh, A. Engineering Early Memory B-Cell-like Phenotype in Hydrogel-Based Immune Organoids. *J. Biomed. Mater. Res. A* **2022**, *110* (8), 1435–1447. https://doi.org/10.1002/jbm.a.37388.
(28) Zhong, Z.; Quiñones-Pérez, M.; Dai, Z.; Juarez, V. M.; Bhatia, E.; Carlson, C. R.; Shah, S. B.; Patel, A.; Fang, Z.; Hu, T.; Allam, M.; Hicks, S. L.; Gupta, M.; Gupta, S. L.; Weeks, E.;

Vagelos, S. D.; Molina, A.; Mulero-Russe, A.; Mora-Boza, A.; Joshi, D. J.; Sekaly, R. P.; Sulchek, T.; Goudy, S. L.; Wrammert, J.; Roy, K.; Boss, J. M.; Coskun, A. F.; Scharer, C. D.; García, A. J.; Koff, J. L.; Singh, A. Human Immune Organoids to Decode B Cell Response in Healthy Donors and Patients with Lymphoma. *Nat. Mater.* **2024**. https://doi.org/10.1038/s41563-024-02037-1.

(29) Liu, H.; Gan, Z.; Qin, X.; Wang, Y.; Qin, J. Advances in Microfluidic Technologies in Organoid Research. *Adv. Healthc. Mater.* **2024**, *13* (21), 2302686. https://doi.org/10.1002/adhm.202302686.

(30) Zushin, P.-J. H.; Mukherjee, S.; Wu, J. C. FDA Modernization Act 2.0: Transitioning beyond Animal Models with Human Cells, Organoids, and AI/ML-Based Approaches. *J. Clin. Invest. 133* (21), e175824. https://doi.org/10.1172/JCI175824.

(31) Low, L. A.; Mummery, C.; Berridge, B. R.; Austin, C. P.; Tagle, D. A. Organs-on-Chips: Into the next Decade. *Nat. Rev. Drug Discov.* **2021**, *20* (5), 345–361. https://doi.org/10.1038/s41573-020-0079-3.

(32) C. Peterson, N.; Kumar Mahalingaiah, P.; Fullerton, A.; Piazza, M. D. Application of Microphysiological Systems in Biopharmaceutical Research and Development. *Lab. Chip* **2020**, *20* (4), 697–708. https://doi.org/10.1039/C9LC00962K.

(33) Birmingham, K. G.; O'Melia, M. J.; Bordy, S.; Aguilar, D. R.; El-Reyas, B.; Lesinski, G.; Thomas, S. N. Lymph Node Subcapsular Sinus Microenvironment-On-A-Chip Modeling Shear Flow Relevant to Lymphatic Metastasis and Immune Cell Homing. *iScience* **2020**, *23* (11). https://doi.org/10.1016/j.isci.2020.101751.

(34) Morrison, A. I.; Sjoerds, M. J.; Vonk, L. A.; Gibbs, S.; Koning, J. J. In Vitro Immunity: An Overview of Immunocompetent Organ-on-Chip Models. *Front. Immunol.* **2024**, *15*. https://doi.org/10.3389/fimmu.2024.1373186.

(35) Hammel, J. H.; Cook, S. R.; Belanger, M. C.; Munson, J. M.; Pompano, R. R. Modeling Immunity In Vitro: Slices, Chips, and Engineered Tissues. *Annu. Rev. Biomed. Eng.* **2021**, *23*, 461–491. https://doi.org/10.1146/annurev-bioeng-082420-124920.

(36) Moura Rosa, P.; Gopalakrishnan, N.; Ibrahim, H.; Haug, M.; Halaas, Ø. The Intercell Dynamics of T Cells and Dendritic Cells in a Lymph Node-on-a-Chip Flow Device. *Lab. Chip* **2016**, *16* (19), 3728–3740. https://doi.org/10.1039/c6lc00702c.

(37) Hammel, J. H.; Arneja, A.; Cunningham, J.; Wang, M.; Schumaecker, S.; Orihuela, Y. M.; Ozulumba, T.; Zatorski, J.; Braciale, T. J.; Luckey, C. J.; Pompano, R. R.; Munson, J. M. Engineered Human Lymph Node Stroma Model for Examining Interstitial Fluid Flow and T Cell Egress. bioRxiv December 7, 2024, p 2024.12.03.622729. https://doi.org/10.1101/2024.12.03.622729.

(38) Kwee, B. J.; Mansouri, M.; Akue, A.; Sung, K. E. On-Chip Human Lymph Node Stromal Network for Evaluating Dendritic Cell and T-Cell Trafficking. *Biofabrication* **2024**, *17* (1), 015009. https://doi.org/10.1088/1758-5090/ad80ce.

(39) Lubitz, A.; Giese, C. Human Artificial Lymph Node (HuALN). In *Encyclopedia of Immunotoxicology*; Vohr, H.-W., Ed.; Springer: Berlin, Heidelberg, 2005; pp 1–6. https://doi.org/10.1007/978-3-642-27786-3_1573-2.

(40) Dauner, A.; Agrawal, P.; Salvatico, J.; Tapia, T.; Dhir, V.; Shaik, S. F.; Drake, D. R.; Byers, A. M. The in Vitro MIMIC® Platform Reflects Age-Associated Changes in Immunological Responses after Influenza Vaccination. *Vaccine* **2017**, *35* (41), 5487–5494. https://doi.org/10.1016/j.vaccine.2017.03.099.

(41) Goyal, G.; Prabhala, P.; Mahajan, G.; Bausk, B.; Gilboa, T.; Xie, L.; Zhai, Y.; Lazarovits, R.; Mansour, A.; Kim, M. S.; Patil, A.; Curran, D.; Long, J. M.; Sharma, S.; Junaid, A.; Cohen, L.; Ferrante, T. C.; Levy, O.; Prantil-Baun, R.; Walt, D. R.; Ingber, D. E. Ectopic Lymphoid Follicle Formation and Human Seasonal Influenza Vaccination Responses Recapitulated in an Organ-on-a-Chip. *Adv. Sci. Weinh. Baden-Wurtt. Ger.* **2022**, *9* (14), e2103241. https://doi.org/10.1002/advs.202103241.

(42) Mazzaglia, C.; Munir, H.; Lei, I. M.; Gerigk, M.; Huang, Y. Y. S.; Shields, J. D. Modeling Structural Elements and Functional Responses to Lymphatic-Delivered Cues in a Murine Lymph Node on a Chip. *Adv. Healthc. Mater.* **2024**, *13* (18), e2303720. https://doi.org/10.1002/adhm.202303720.
(43) Jeger-Madiot, R.; Planas, D.; Staropoli, I.; Debarnot, H.; Kervevan, J.; Mary, H.; Collina, C.; Fonseca, B. F.; Robinot, R.; Gellenoncourt, S.; Schwartz, O.; Ewart, L.; Bscheider, M.; Gobaa, S.; Chakrabarti, L. A. Modeling Memory B Cell Responses in a Lymphoid Organ-Chip to Evaluate mRNA Vaccine Boosting. *J. Exp. Med.* **2024**, *221* (10), e20240289. https://doi.org/10.1084/jem.20240289.
(44) Ortiz-Cárdenas, J. E.; Zatorski, J. M.; Arneja, A.; Montalbine, A. N.; Munson, J. M.; Luckey, C. J.; Pompano, R. R. Towards Spatially-Organized Organs-on-Chip: Photopatterning Cell-Laden Thiol-Ene and Methacryloyl Hydrogels in a Microfluidic Device. *Organs---Chip* **2022**, *4*, 100018. https://doi.org/10.1016/j.ooc.2022.100018.
(45) Hallfors, N.; Shanti, A.; Sapudom, J.; Teo, J.; Petroianu, G.; Lee, S.; Planelles, L.; Stefanini, C. Multi-Compartment Lymph-Node-on-a-Chip Enables Measurement of Immune Cell Motility in Response to Drugs. *Bioengineering* **2021**, *8* (2), 19. https://doi.org/10.3390/bioengineering8020019.
(46) Shanti, A.; Samara, B.; Abdullah, A.; Hallfors, N.; Accoto, D.; Sapudom, J.; Alatoom, A.; Teo, J.; Danti, S.; Stefanini, C. Multi-Compartment 3D-Cultured Organ-on-a-Chip: Towards a Biomimetic Lymph Node for Drug Development. *Pharmaceutics* **2020**, *12* (5), 464.
(47) Germann, A.; Schulz, J. C.; Kemp-Kamke, B.; Zimmermann, H.; von Briesen, H. Standardized Serum-Free Cryomedia Maintain Peripheral Blood Mononuclear Cell Viability, Recovery, and Antigen-Specific T-Cell Response Compared to Fetal Calf Serum-Based Medium. *Biopreservation Biobanking* **2011**, *9* (3), 229–236. https://doi.org/10.1089/bio.2010.0033.
(48) Coradin, T.; Wang, K.; Law, T.; Trichet, L. Type I Collagen-Fibrin Mixed Hydrogels: Preparation, Properties and Biomedical Applications. *Gels* **2020**, *6* (4), 36. https://doi.org/10.3390/gels6040036.
(49) Logie, C.; van Schaik, T.; Pompe, T.; Pietsch, K. Fibronectin-Functionalization of 3D Collagen Networks Supports Immune Tolerance and Inflammation Suppression in Human Monocyte-Derived Macrophages. *Biomaterials* **2021**, *268*, 120498. https://doi.org/10.1016/j.biomaterials.2020.120498.
(50) P. Huang, C.; Lu, J.; Seon, H.; P. Lee, A.; A. Flanagan, L.; Kim, H.-Y.; J. Putnam, A.; Li Jeon, N. Engineering Microscale Cellular Niches for Three-Dimensional Multicellular Co-Cultures. *Lab. Chip* **2009**, *9* (12), 1740–1748. https://doi.org/10.1039/B818401A.
(51) Wan, Z.; Zhong, A. X.; Zhang, S.; Pavlou, G.; Coughlin, M. F.; Shelton, S. E.; Nguyen, H. T.; Lorch, J. H.; Barbie, D. A.; Kamm, R. D. A Robust Method for Perfusable Microvascular Network Formation In Vitro. *Small Methods* **2022**, *6* (6), 2200143. https://doi.org/10.1002/smtd.202200143.
(52) Huang, C. P.; Lu, J.; Seon, H.; Lee, A. P.; Flanagan, L. A.; Kim, H.-Y.; Putnam, A. J.; Jeon, N. L. Engineering Microscale Cellular Niches for Three-Dimensional Multicellular Co-Cultures. *Lab. Chip* **2009**, *9* (12), 1740–1748.
(53) Dornhof, J.; Kieninger, J.; Muralidharan, H.; Maurer, J.; A. Urban, G.; Weltin, A. Microfluidic Organ-on-Chip System for Multi-Analyte Monitoring of Metabolites in 3D Cell Cultures. *Lab. Chip* **2022**, *22* (2), 225–239. https://doi.org/10.1039/D1LC00689D.
(54) Miranda, I.; Souza, A.; Sousa, P.; Ribeiro, J.; Castanheira, E. M. S.; Lima, R.; Minas, G. Properties and Applications of PDMS for Biomedical Engineering: A Review. *J. Funct. Biomater.* **2022**, *13* (1), 2. https://doi.org/10.3390/jfb13010002.
(55) Stachowiak, A. N.; Irvine, D. J. Inverse Opal Hydrogel-Collagen Composite Scaffolds as a Supportive Microenvironment for Immune Cell Migration. *J. Biomed. Mater. Res. A* **2008**, *85A* (3), 815–828. https://doi.org/10.1002/jbm.a.31661.

(56) Locci, M.; Wu, J.; Arumemi, F.; Mikulski, Z.; Dahlberg, C.; Miller, A. T.; Crotty, S. Activin A Programs Human TFH Cell Differentiation. *Nat. Immunol.* **2016**, *17* (8), 976. https://doi.org/10.1038/ni.3494.
(57) Good, K. L.; Avery, D. T.; Tangye, S. G. Resting Human Memory B Cells Are Intrinsically Programmed for Enhanced Survival and Responsiveness to Diverse Stimuli Compared to Naive B Cells1. *J. Immunol.* **2009**, *182* (2), 890–901. https://doi.org/10.4049/jimmunol.182.2.890.
(58) Zheng, J.; Liu, Y.; Qin, G.; Lam, K.-T.; Guan, J.; Xiang, Z.; Lewis, D. B.; Lau, Y.-L.; Tu, W. Generation of Human Th1-like Regulatory CD4+ T Cells by an Intrinsic IFN-γ- and T-Bet-Dependent Pathway. *Eur. J. Immunol.* **2011**, *41* (1), 128–139. https://doi.org/10.1002/eji.201040724.
(59) Majedi, F. S.; Hasani-Sadrabadi, M. M.; Thauland, T. J.; Li, S.; Bouchard, L.-S.; Butte, M. J. T-Cell Activation Is Modulated by the 3D Mechanical Microenvironment. *Biomaterials* **2020**, *252*, 120058. https://doi.org/10.1016/j.biomaterials.2020.120058.
(60) Belanger, M. C.; Ball, A. G.; Catterton, M. A.; Kinman, A. W. L.; Anbaei, P.; Groff, B. D.; Melchor, S. J.; Lukens, J. R.; Ross, A. E.; Pompano, R. R. Acute Lymph Node Slices Are a Functional Model System to Study Immunity Ex Vivo. *ACS Pharmacol. Transl. Sci.* **2021**, *4* (1), 128–142. https://doi.org/10.1021/acsptsci.0c00143.
(61) Groff, B. D.; Kinman, A. W. L.; Woodroof, J. F.; Pompano, R. R. Immunofluorescence Staining of Live Lymph Node Tissue Slices. *J. Immunol. Methods* **2019**, *464*, 119–125. https://doi.org/10.1016/j.jim.2018.10.010.
(62) Piccinini, F.; Kiss, A.; Horvath, P. CellTracker (Not Only) for Dummies. *Bioinformatics* **2016**, *32* (6), 955–957. https://doi.org/10.1093/bioinformatics/btv686.